galaxies

MDPI

Article

Signatures of Lorentz Violation in Continuous Gravitational-Wave Spectra of Ellipsoidal Neutron Stars

Rui Xu [1,*], Yong Gao [1,2] and Lijing Shao [1,3,*]

[1] Kavli Institute for Astronomy and Astrophysics, Peking University, Beijing 100871, China
[2] Department of Astronomy, School of Physics, Peking University, Beijing 100871, China; gaoyong.physics@pku.edu.cn
[3] National Astronomical Observatories, Chinese Academy of Sciences, Beijing 100012, China
* Correspondence: xuru@pku.edu.cn (R.X.); lshao@pku.edu.cn (L.S.)

Abstract: We studied the effects of the Lorentz invariance violation on the rotation of neutron stars (NSs) in the minimal gravitational Standard-Model Extension framework, and calculated the quadrupole radiation generated by them. Aiming at testing Lorentz invariance with observations of continuous gravitational waves (GWs) from rotating NSs in the future, we compared the GW spectra of a rotating ellipsoidal NS under Lorentz-violating gravity with those of a Lorentz-invariant one. The former were found to possess frequency components higher than the second harmonic, which does not happen for the latter, indicating those higher frequency components to be potential signatures of Lorentz violation in continuous GW spectra of rotating NSs.

Keywords: Lorentz violation; Standard-Model Extension

Citation: Xu, R.; Gao, Y.; Shao, L. Signatures of Lorentz Violation in Continuous Gravitational-Wave Spectra of Ellipsoidal Neutron Stars. *Galaxies* **2021**, *9*, 12. https://doi.org/10.3390/galaxies9010012

Academic Editor: Marco Schreck
Received: 5 January 2021
Accepted: 25 January 2021
Published: 29 January 2021

1. Introduction

The observation of gravitational waves (GWs) from the compact binary system GW170817 initiates the era of multimessenger astronomy [1,2]. Gravitational theories, including the renowned general relativity (GR), are being exposed to unprecedented tests utilizing GW signals [3]. Lorentz invariance, incorporated locally in GR and many other alternative gravitational theories, is certainly one of the fundamental principles subjected to these tests [4–8]. By employing the Standard-Model Extension (SME) framework [9–13], which is widely used to investigate consequences from possible violations of Lorentz invariance in terrestrial experiments and astrophysical observations [14], stringent bounds have been set for the coefficients for Lorentz violation in the gravitational sector of the SME framework after analyzing the observed GW data [2,5–7].

Besides the coalescence of compact binary systems, GW sources of another type are deformed rotating neutron stars (NSs). In particular, when the angular velocity of a deformed NS is misaligned with its angular momentum, the star precesses about the direction of the angular momentum, radiating out GWs continuously [15,16]. The search for such continuous GW signals is ongoing [17–22]. Once detected, the continuous GW signals will tell us a substantial piece of information on NS structure and deformability. Furthermore, they will bring new tests for the laws of physics, among which lies Lorentz invariance as one of the fundamental principles (see e.g., [8]).

To test Lorentz invariance, an investigation of the scenario where it is violated is necessary. The effects of Lorentz violation on rotating spheroidal stars are studied in detail in [23] under the minimal gravitational SME framework. The modification to the free precession of a deformed star is depicted by the term "twofold precession," as briefly speaking, Lorentz violation causes the angular momentum to precess about a fixed direction while at the same time the star still precesses about the instantaneous direction of the angular momentum. The correction in the quadrupole radiation due to the modification of the rotation of the star was calculated in [23], and it was found that the quadrupole

radiation from a spheroidal star affected by Lorentz violation has frequency components over double the frequency of the fundamental one.

In this work, we extend the numerical results in [23] to ellipsoidal NSs. The characteristically higher harmonics due to Lorentz violation remain in the GW spectra, as we expected. More importantly, our numerical calculation for the quadrupole radiation from an ellipsoidal NS in the absence of Lorentz violation indicates that though the nonaxisymmetry of the star modulates the first and the second harmonics in the GW spectra, as discussed in [16,24,25], it does not generate harmonics higher than the second for freely precessing NSs. Therefore, harmonics higher than the second are indeed possible signatures for Lorentz violation in the GW spectra of rotating solitary NSs.

We organize the paper as follows. In Section 2, we present the analytical equations to construct the quadrupole radiation from a rotating ellipsoid under Lorentz-violating gravity. Then in Section 3, numerical solutions to the rotation equations for ellipsoids with uniform density are obtained and used to construct examples of the quadrupole radiation. Subsequently, Fourier transformations are performed to extract the frequency components of the quadrupole GWs, and we show that while the GW from an ellipsoid under the twofold precession contains harmonics higher than the second, the GW from an ellipsoid under free precession only has frequencies around the first and the second harmonics. In the end, the conclusions are summarized in Section 4. For simplicity in writing equations, we use the geometrized unit system where $G = c = 1$. However, standard units do appear when numerical estimations are desired for realistic NSs.

2. Theoretical Basics

To proceed with the calculation, we neglect relativistic corrections to the NS's structure and motion, and solve its motion from the rotation equations for rigid bodies.[1] Assuming that in the body frame x–y–z, the surface of the star is described by

$$\frac{x^2}{a_x^2} + \frac{y^2}{a_y^2} + \frac{z^2}{a_z^2} = 1, \tag{1}$$

with semi-axes a_x, a_y and a_z, then the Lagrangian for the rotation of the star can be written as

$$L = \frac{1}{2}\left(I^{xx}(\Omega^x)^2 + I^{yy}(\Omega^y)^2 + I^{zz}(\Omega^z)^2\right) - \delta U, \tag{2}$$

where I^{xx}, I^{yy} and I^{zz} are the eigenvalues of the moment of inertia tensor along the principal axes, and Ω^x, Ω^y and Ω^z are the components of the angular velocity of the star in the x–y–z frame. The orientation-dependent self-energy δU is calculated from the anisotropic correction $\delta\Phi$ to the Newtonian potential Φ in the minimal gravitational SME, namely [13],

$$\begin{aligned} \delta\Phi &= -\frac{1}{2}\bar{s}^{ij}\int \frac{(x^i - x'^i)(x^j - x'^j)}{|\boldsymbol{x} - \boldsymbol{x}'|^3}\rho(\boldsymbol{x}')\mathrm{d}^3\boldsymbol{x}', \\ \delta U &= -\frac{1}{4}\bar{s}^{ij}\int \frac{(x^i - x'^i)(x^j - x'^j)}{|\boldsymbol{x} - \boldsymbol{x}'|^3}\rho(\boldsymbol{x})\rho(\boldsymbol{x}')\mathrm{d}^3\boldsymbol{x}\,\mathrm{d}^3\boldsymbol{x}', \end{aligned} \tag{3}$$

where $\bar{s}^{ij}$, with $i, j = x, y, z$, are the coefficients for Lorentz violation in the body frame [12,13], and ρ is the density of the star.

In the SME framework, the coefficients for Lorentz violation are assumed to be constant in inertial frames. Therefore, as the star rotates, the coefficients $\bar{s}^{ij}$ depend on the orientation of the star according to

$$\bar{s}^{ij} = R^{iI}R^{jJ}\bar{s}^{IJ}, \tag{4}$$

[1] Relativistic corrections are reasonably characterized by the compactness of the body, which is about 0.1 for a NS.

where R^{iI} represents the rotation matrix transforming an inertial frame X–Y–Z to the body frame x–y–z. The capital indices run over X, Y and Z, and $\bar{s}^{IJ}$ are constant coefficients for Lorentz violation. The orientation dependence of $\bar{s}^{ij}$, originated from the rotation matrix, can be easily described by the Euler angles (α, β, γ) in Figure 1, as the rotation matrix in terms of the Euler angles is

$$R^{iI} = \begin{matrix} \\ i \\ \\ \downarrow \end{matrix} \overset{\longrightarrow}{I} \begin{pmatrix} \cos\alpha\cos\gamma - \sin\alpha\cos\beta\sin\gamma & \sin\alpha\cos\gamma + \cos\alpha\cos\beta\sin\gamma & \sin\beta\sin\gamma \\ -\cos\alpha\sin\gamma - \sin\alpha\cos\beta\cos\gamma & -\sin\alpha\sin\gamma + \cos\alpha\cos\beta\cos\gamma & \sin\beta\cos\gamma \\ \sin\alpha\sin\beta & -\cos\alpha\sin\beta & \cos\beta \end{pmatrix}. \tag{5}$$

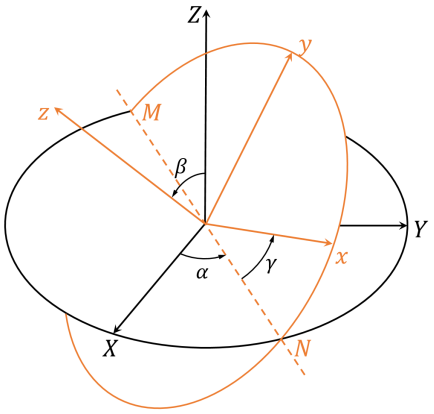

Figure 1. Euler angles transforming the X–Y–Z inertial frame to the x–y–z body frame. First, rotate the X–Y–Z frame about the Z axis with angle α so that the X-axis aligns with the intersection line MN. Then, rotate the just obtained X–Y–Z frame about the line MN with angle β so that the Z-axis aligns with the z-axis. Last, rotate the new X–Y–Z frame about the z-axis with angle γ so that it overlaps with the x–y–z frame.

Together with the relations between the velocity components and the Euler angles [26],

$$\begin{aligned} \Omega^x &= \dot{\alpha}\sin\beta\sin\gamma + \dot{\beta}\cos\gamma, \\ \Omega^y &= \dot{\alpha}\sin\beta\cos\gamma - \dot{\beta}\sin\gamma, \\ \Omega^z &= \dot{\alpha}\cos\beta + \dot{\gamma}, \end{aligned} \tag{6}$$

where dots denote time derivatives, the Euler–Lagrange equations for the Euler angles can be obtained from the Lagrangian (2). Given the shape and density of the star, the moment of inertia tensor and the integrals in δU can be calculated, and then the Euler angles can be solved to describe the rotation of the star.

Once the rotation of the star is known, its gravitational quadrupole radiation can be calculated via the metric perturbation

$$h^{IJ} = -\frac{2}{r}\ddot{I}^{IJ}, \tag{7}$$

where r is the distance from the distant star to the observer, and the double dots denote the second time derivative. In [23], it is shown that $\ddot{I}^{IJ}$ can be written as

$$\ddot{I}^{IJ} = R^{iI}R^{jJ}A^{ij}, \tag{8}$$

with the body-frame quantities A^{ij} being

$$\begin{aligned}
A^{xx} &= 2\Big(\Delta_2(\Omega^y)^2 - \Delta_3(\Omega^z)^2\Big),\\
A^{yy} &= 2\Big(\Delta_3(\Omega^z)^2 - \Delta_1(\Omega^x)^2\Big),\\
A^{zz} &= 2\Big(\Delta_1(\Omega^x)^2 - \Delta_2(\Omega^y)^2\Big),\\
A^{xy} &= \left(\frac{(\Delta_3)^2}{I^{zz}} + \Delta_1 - \Delta_2\right)\Omega^x\Omega^y + \frac{\Delta_3}{I^{zz}}\Gamma^z,\\
A^{xz} &= \left(\frac{(\Delta_2)^2}{I^{yy}} + \Delta_3 - \Delta_1\right)\Omega^x\Omega^z + \frac{\Delta_2}{I^{yy}}\Gamma^y,\\
A^{yz} &= \left(\frac{(\Delta_1)^2}{I^{xx}} + \Delta_2 - \Delta_3\right)\Omega^y\Omega^z + \frac{\Delta_1}{I^{xx}}\Gamma^x,
\end{aligned} \tag{9}$$

for any rigid body subjected to arbitrary rotations. The quantities Δ_1, Δ_2 and Δ_3 are defined as

$$\Delta_1 = I^{yy} - I^{zz}, \quad \Delta_2 = I^{zz} - I^{xx}, \quad \Delta_3 = I^{xx} - I^{yy}, \tag{10}$$

and the components of the torque, Γ^x, Γ^y and Γ^z, are calculated from the orientation-dependent self-energy δU via

$$\begin{aligned}
\Gamma^x &= -\frac{\sin\gamma}{\sin\beta}\,\partial_\alpha\delta U - \cos\gamma\,\partial_\beta\delta U + \cot\beta\sin\gamma\,\partial_\gamma\delta U,\\
\Gamma^y &= -\frac{\cos\gamma}{\sin\beta}\,\partial_\alpha\delta U + \sin\gamma\,\partial_\beta\delta U + \cot\beta\cos\gamma\,\partial_\gamma\delta U,\\
\Gamma^z &= -\partial_\gamma\delta U.
\end{aligned} \tag{11}$$

Finally, the two physical degrees of freedom in the GW can be extracted from h^{IJ} by defining the plus and the cross modes for an observer whose colatitude and azimuth are θ_o and ϕ_o in the X–Y–Z frame [27],

$$\begin{aligned}
h_+ &= \frac{1}{2}\Big(\hat\theta_o^I\hat\theta_o^J - \hat\phi_o^I\hat\phi_o^J\Big)h^{IJ} = -\frac{1}{r}\Big(\hat\theta_o^I\hat\theta_o^J - \hat\phi_o^I\hat\phi_o^J\Big)\ddot I^{IJ},\\
h_\times &= \frac{1}{2}\Big(\hat\theta_o^I\hat\phi_o^J + \hat\phi_o^I\hat\theta_o^J\Big)h^{IJ} = -\frac{1}{r}\Big(\hat\theta_o^I\hat\phi_o^J + \hat\phi_o^I\hat\theta_o^J\Big)\ddot I^{IJ},
\end{aligned} \tag{12}$$

where $\hat\theta_o^I$ and $\hat\phi_o^I$ are the XYZ-components of the transverse unit vectors

$$\begin{aligned}
\hat{\boldsymbol\theta}_o &= \cos\theta_o\cos\phi_o\,\hat{\boldsymbol e}_X + \cos\theta_o\sin\phi_o\,\hat{\boldsymbol e}_Y - \sin\theta_o\hat{\boldsymbol e}_Z,\\
\hat{\boldsymbol\phi}_o &= -\sin\phi_o\,\hat{\boldsymbol e}_X + \cos\phi_o\,\hat{\boldsymbol e}_Y.
\end{aligned} \tag{13}$$

Note that $\hat{\boldsymbol e}_X$, $\hat{\boldsymbol e}_Y$ and $\hat{\boldsymbol e}_Z$ are the unit vectors of the X–Y–Z frame, and $\hat{\boldsymbol e}_x$, $\hat{\boldsymbol e}_y$ and $\hat{\boldsymbol e}_z$ will be used as the unit vectors of the x–y–z frame.

3. Numerical Examples

Now we can use the above equations to numerically calculate the GW spectra of a rotating ellipsoidal NS affected by Lorentz violation. To simplify the calculation of δU, we assume the density of the star to be constant. Extension to realistic nonuniform NSs is straightforward. The advantage of using a constant density is that the angular parts of the integrals in δU can be carried out analytically. Specifically speaking, define

$$U^{ij} := \frac{1}{2}\int\frac{\big(x^i - x'^i\big)\big(x^j - x'^j\big)}{|\boldsymbol x - \boldsymbol x'|^3}\rho(\boldsymbol x)\rho(\boldsymbol x')\mathrm{d}^3\boldsymbol x\,\mathrm{d}^3\boldsymbol x'; \tag{14}$$

then they are related to the Newtonian potential

$$\Phi = -\int \frac{\rho(\boldsymbol{x}')}{|\boldsymbol{x}-\boldsymbol{x}'|}\mathrm{d}^3\boldsymbol{x}', \tag{15}$$

via

$$U^{ij} = \int \rho(\boldsymbol{x}) x^i \partial_j \Phi \mathrm{d}^3\boldsymbol{x}. \tag{16}$$

The Newtonian potential of a uniform ellipsoid is known to be [27,28]

$$\Phi = -\pi\rho\Big(A_0 - A_x x^2 - A_y y^2 - A_z z^2\Big), \tag{17}$$

where

$$\begin{aligned} A_0 &= a_x a_y a_z \int_0^\infty \frac{\mathrm{d}u}{\sqrt{(a_x^2+u)(a_y^2+u)(a_z^2+u)}}, \\ A_i &= a_x a_y a_z \int_0^\infty \frac{\mathrm{d}u}{(a_i^2+u)\sqrt{(a_x^2+u)(a_y^2+u)(a_z^2+u)}}, \end{aligned} \tag{18}$$

with $i = x, y, z$. Consequently, the nonvanishing U^{ij} are found to be

$$U^{xx} = \frac{8\pi^2}{15}\rho^2 A_x a_x^3 a_y a_z, \quad U^{yy} = \frac{8\pi^2}{15}\rho^2 A_y a_x a_y^3 a_z, \quad U^{zz} = \frac{8\pi^2}{15}\rho^2 A_z a_x a_y a_z^3. \tag{19}$$

For NSs, the density varies from the center to the surface. For our purposes, we take a uniform density of $10^{15}\,\mathrm{g/cm^3}$ in numerical calculations. As for the semi-axes, because NSs are compact objects having tiny deformations if any, we can only say that they are all about 10 km, roughly the radius of a spherical NS predicted by GR. The most often used parameters to characterize NS deformation are the oblateness ϵ and the nonaxisymmetry δ. They are defined as

$$\epsilon = \frac{I^{zz} - I^{xx}}{I^{xx}}, \quad \delta = \frac{I^{yy} - I^{xx}}{I^{zz} - I^{xx}}, \tag{20}$$

with an assumption that I^{zz} is the largest eigenvalue of the moment of inertia tensor. NS models have suggested that ϵ is less than 10^{-7} [29], while the magnitude of δ is hardly known. For demonstration, we take 0.1 for both ϵ and δ in the following numerical examples. In addition, we use 10 km for a_z, and then the values of a_x and a_y are determined by noticing

$$I^{xx} = \frac{4\pi}{15}\rho a_x a_y a_z (a_y^2 + a_z^2), \quad I^{yy} = \frac{4\pi}{15}\rho a_x a_y a_z (a_x^2 + a_z^2), \quad I^{zz} = \frac{4\pi}{15}\rho a_x a_y a_z (a_x^2 + a_y^2), \tag{21}$$

for uniform ellipsoids.

Then to compute δU as a function of the Euler angles, we take numerical values $\bar{s}^{XX} = 0.02$, $\bar{s}^{YY} = 0.01$, $\bar{s}^{ZZ} = -0.04$ and $\bar{s}^{XY} = \bar{s}^{XZ} = \bar{s}^{YZ} = 0$ for the coefficients for Lorentz violation in the inertial frame. This means that the axes of the inertial frame are the principal axes of the $\bar{s}^{ij}$ tensor. Note that this is a theoretical inertial frame fixed by the coefficients for Lorentz violation. It generally does not coincide with the widely used experimental inertial frame, namely, the Sun-centered celestial-equatorial frame defined in [11].

All the parameters in the Lagrangian (2) have been set now. Numerical solutions for the Euler angles can be obtained once initial values are given. For numerical calculations,

a dimensionless parametrization for the angular velocities is helpful. This can be achieved by employing a time unit. To be consistent with the choice in [23], it is taken to be

$$t_c := \sqrt{\frac{2I^{xx}}{U^{yy} - U^{zz}}}. \tag{22}$$

For a uniform ellipsoid, while keeping only the leading contributions from ϵ and δ, it is

$$t_c = \sqrt{\frac{a_y^2 + a_z^2}{\pi\rho\left(A_y a_y^2 - A_z a_z^2\right)}} \approx \sqrt{\frac{15}{4\pi\rho\epsilon(1-\delta)}} \sim 10^{-3}\,\mathrm{s}, \tag{23}$$

where the magnitude estimation is made for $\rho = 10^{15}\,\mathrm{g/cm^3}$ and $\epsilon = \delta = 0.1$. Therefore, a dimensionless angular velocity at order unity in our numerical results corresponds to about 1000 rad/s.

Figure 2 shows the trajectories of the tail of the unit vector $\hat{\boldsymbol{e}}_z$ in the inertial frame to intuitively illustrate the rotations of the star for a certain set of initial values. Our examples consist of two solutions: the plot on the left shows a twofold precession with $\bar{s}^{IJ}$ taking the above values, and the plot on the right shows a free precession without Lorentz violation for comparison. The distinction is also reflected by the trajectories of the tail of the angular momentum unit vector: in the left plot, there is a nontrivial trajectory for the angular momentum unit vector, and in the right plot the angular momentum unit vector does not change with time.

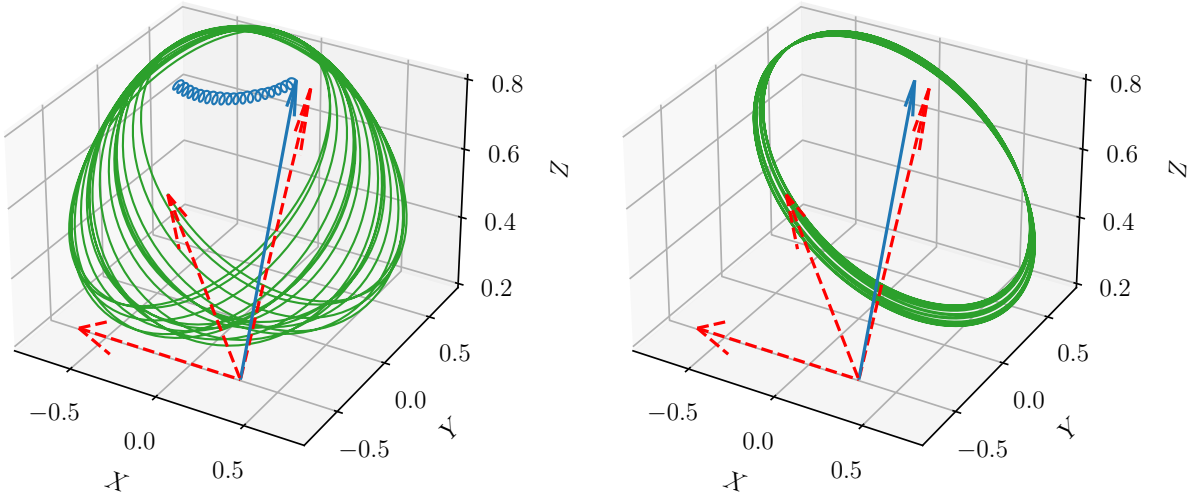

Figure 2. Illustrations for an example of the Lorentz-violating twofold precession (**left**) and an example of the Lorentz-invariant free precession (**right**). The green trajectories trace the tail of the body-frame unit vector $\hat{\boldsymbol{e}}_z$ in the inertial frame, while the blue trajectory in the left plot traces the tail of the angular momentum unit vector in the inertial frame. The red arrows are the body-frame unit vectors $\hat{\boldsymbol{e}}_x$, $\hat{\boldsymbol{e}}_y$ and $\hat{\boldsymbol{e}}_z$ at $t = 0$, while the blue arrows indicate the angular momentum unit vector at $t = 0$. The angular momentum is conserved in free precessions so the blue arrow in the right plot remains unchanged with time. The initial values for both solutions are $\alpha|_{t=0} = 0$, $\beta|_{t=0} \approx 0.762$, $\gamma|_{t=0} = \pi/2$, $\dot{\alpha}|_{t=0} \approx 1.26$, $\dot{\beta}|_{t=0} = 0.5$ and $\dot{\gamma}|_{t=0} \approx 0.0449$. Time and time derivatives are dimensionless under the time unit t_c given by Equation (23).

With the two solutions, we calculated the GWs according to Equation (12) for an observer at $\theta_o = 0.8$ rad and $\phi_o = 0$. The results are presented in Figure 3. Their Fourier transformations are shown in Figure 4; only the plus mode is shown, as the cross mode has very much the same spectra. The spectrum of the free precession shows a fundamental angular frequency at about $1.4/t_c$, and peaks around the second harmonic at about $2.9/t_c$. We know that if the star is axisymmetric, free precessions generate GWs having exactly two frequencies, with one being twice the other. The nonaxisymmetry here modulates both the fundamental frequency and the second harmonic. This has been discussed in

references [16,24,25]. What we are showing in the left plot of Figure 4 tells us that the twofold precession, namely, the rotation of an otherwise freely precessing NS under Lorentz-violating gravity, generates similar GW frequency components. However, more interestingly, in the enlarged plot on the right, we clearly see the distinction that while the twofold precession generates frequency components around the third harmonic, the free precession has no component of the third harmonic at all. Higher frequency components exist in the spectra of the Lorentz-violating twofold precession, but they can easily be missed as they are too small.

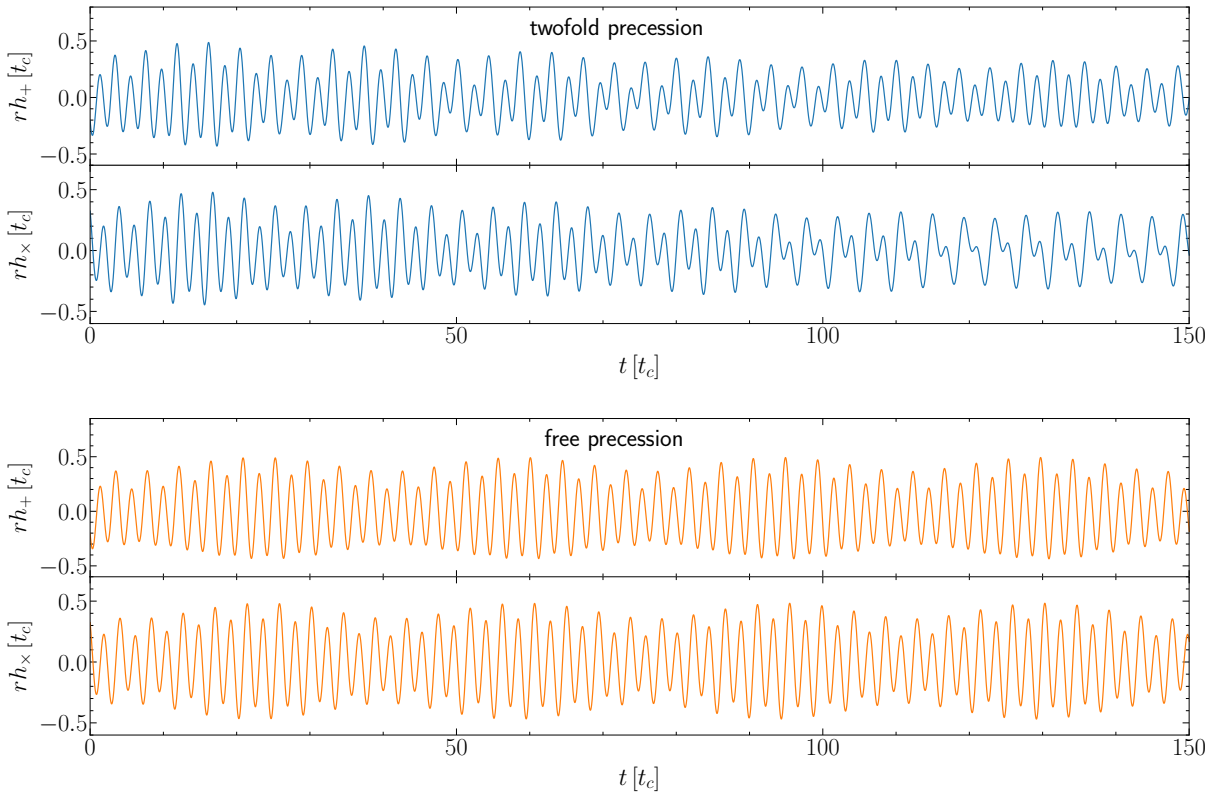

Figure 3. GWs from a rigid body undergoing the rotations in Figure 2. The observer receiving the waves has colatitude $\theta_o = 0.8$ rad and azimuth $\phi_o = 0$ in the X–Y–Z frame. The geometrized unit of time and distance is the time unit t_c given by Equation (23).

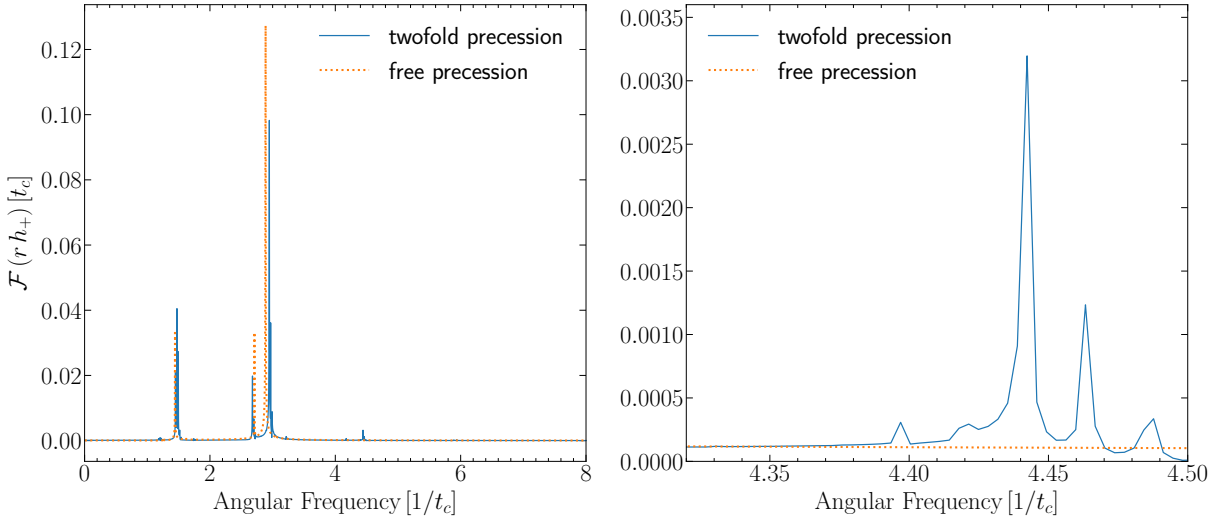

Figure 4. Fourier transformations of the rh_+ waves in Figure 3. The two noticeable peaks at about 1.4 and 2.9 in the left plot are the first and the second harmonics for both twofold precession and free precession. The modulation due to nonaxisymmetry is clearly represented by the adjacent peak at about 2.7 close to the second harmonic for both kinds of motion. However, the barely visible tiny peaks, reflecting modulations due to Lorentz violation, only exist for twofold precession. The right plot, which zooms in on the tiny peak between 4 and 5, demonstrates the point. Note that in the plots the geometrized unit of Fourier amplitude is t_c, and the geometrized unit of angular frequency is $1/t_c$.

4. Conclusions

We have presented the analytical formulae to calculate the rotation of NSs under Lorentz-violating gravity in the minimal gravitational SME framework, and to construct the quadrupole GWs emitted from these NSs. Numerical examples were plotted to demonstrate our conclusion that while freely precessing NSs in the Lorentz-invariant gravity do not emit quadrupole GWs at frequencies higher than the second harmonic, NSs undergoing the twofold precession due to Lorentz violation do. Therefore, harmonics higher than the second in the spectra of continuous GWs are appealing signatures of Lorentz violation. Once continuous GWs from rotating NSs are detected, a potential test of Lorentz invariance can be performed by examining harmonics higher than the second in the spectra. However, we do notice a possible difficulty in this test: there might be conventional torques, such as the electromagnetic spin-down torque [30–33], acting on the NS to cause similar twofold precession motions and to generate higher harmonics in the GW spectra. Although the questions of whether the twofold precession caused by Lorentz violation can be distinguished from rotations of NSs under the electromagnetic spin-down torque and whether the GW spectra of the latter have frequency components higher than the second harmonic lie beyond the scope of this work, they are certainly worth being investigated further. Furthermore, a statistical study of continuous GWs from an ensemble of NSs might have the potential to distinguish between the two scenarios, as the Lorentz violation is universal for all NSs, and the astrophysical torques are different for different systems.

Author Contributions: Conceptualization, L.S.; formal analysis, R.X.; writing—original draft preparation, R.X.; writing—review and editing, Y.G. and L.S.; visualization, Y.G. and R.X.; funding acquisition, L.S. All authors have read and agreed to the published version of the manuscript.

Funding: This work was supported by the National Natural Science Foundation of China (11975027, 11991053, 11721303), the National SKA Program of China (2020SKA0120300), the Young Elite Scientists Sponsorship Program by the China Association for Science and Technology (2018QNRC001), the Max Planck Partner Group Program funded by the Max Planck Society and the High-Performance Computing Platform of Peking University. It was partially supported by the Strategic Priority Research Program of the Chinese Academy of Sciences through the grant number XDB23010200. R.X. is supported by the Boya Postdoctoral Fellowship at Peking University.

Acknowledgments: We are grateful to Marco Schreck for the invitation to submit an article to this special issue.

Conflicts of Interest: The authors declare no conflict of interest.

References

1. Abbott, B.P.; Abbott, R.; Abbott, T.D.; Acernese, F.; Ackley, K.; Adams, C.; Adams, T.; Addesso, P.; Adhikari, R.X.; Adya, V.B.; et al. Multi-messenger Observations of a Binary Neutron Star Merger. *Astrophys. J. Lett.* **2017**, *848*, L12. [CrossRef]
2. Abbott, B.P.; Abbott, R.; Abbott, T.D.; Acernese, F.; Ackley, K.; Adams, C.; Adams, T.; Addesso, P.; Adhikari, R.X.; Adya, V.B.; et al. Gravitational Waves and Gamma-rays from a Binary Neutron Star Merger: GW170817 and GRB 170817A. *Astrophys. J. Lett.* **2017**, *848*, L13. [CrossRef]
3. Corda, C. Interferometric detection of gravitational waves: The definitive test for General Relativity. *Int. J. Mod. Phys. D* **2009**, *18*, 2275–2282. [CrossRef]
4. Mirshekari, S.; Yunes, N.; Will, C.M. Constraining Generic Lorentz Violation and the Speed of the Graviton with Gravitational Waves. *Phys. Rev. D* **2012**, *85*, 024041. [CrossRef]
5. Kostelecký, V.A.; Mewes, M. Testing local Lorentz invariance with gravitational waves. *Phys. Lett. B* **2016**, *757*, 510–514. [CrossRef]
6. Shao, L. Combined search for anisotropic birefringence in the gravitational-wave transient catalog GWTC-1. *Phys. Rev. D* **2020**, *101*, 104019. [CrossRef]
7. Liu, X.; He, V.F.; Mikulski, T.M.; Palenova, D.; Williams, C.E.; Creighton, J.; Tasson, J.D. Measuring the speed of gravitational waves from the first and second observing run of Advanced LIGO and Advanced Virgo. *Phys. Rev. D* **2020**, *102*, 024028. [CrossRef]
8. Xu, R.; Zhao, J.; Shao, L. Neutron Star Structure in the Minimal Gravitational Standard-Model Extension and the Implication to Continuous Gravitational Waves. *Phys. Lett. B* **2020**, *803*, 135283. [CrossRef]
9. Colladay, D.; Kostelecký, V.A. CPT violation and the standard model. *Phys. Rev. D* **1997**, *55*, 6760–6774. [CrossRef]
10. Colladay, D.; Kostelecký, V.A. Lorentz violating extension of the standard model. *Phys. Rev. D* **1998**, *58*, 116002. [CrossRef]
11. Kostelecký, V.A.; Mewes, M. Signals for Lorentz violation in electrodynamics. *Phys. Rev. D* **2002**, *66*, 056005. [CrossRef]
12. Kostelecký, V.A. Gravity, Lorentz violation, and the standard model. *Phys. Rev. D* **2004**, *69*, 105009. [CrossRef]
13. Bailey, Q.G.; Kostelecký, V.A. Signals for Lorentz violation in post-Newtonian gravity. *Phys. Rev. D* **2006**, *74*, 045001. [CrossRef]
14. Kostelecký, V.A.; Russell, N. Data Tables for Lorentz and CPT Violation. *Rev. Mod. Phys.* **2011**, *83*, 11–31. [CrossRef]
15. Zimmermann, M.; Szedenits, E. Gravitational waves from rotating and precessing rigid bodies: Simple models and applications to pulsars. *Phys. Rev. D* **1979**, *20*, 351–355. [CrossRef]
16. Zimmermann, M. Gravitational waves from rotating and precessing rigid bodies. 1. general solutions and computationally useful formulas. *Phys. Rev. D* **1980**, *21*, 891–898. [CrossRef]
17. Abbott, B.P.; Abbott, R.; Abbott, T.D.; Acernese, F.; Ackley, K.; Adams, C.; Adams, T.; Addesso, P.; Adhikari, R.X.; Adya, V.B.; et al. All-sky search for continuous gravitational waves from isolated neutron stars using Advanced LIGO O2 data. *Phys. Rev. D* **2019**, *100*, 024004. [CrossRef]
18. Covas, P.B.; Sintes, A.M. First all-sky search for continuous gravitational-wave signals from unknown neutron stars in binary systems using Advanced LIGO data. *Phys. Rev. Lett.* **2020**, *124*, 191102. [CrossRef]
19. Dergachev, V.; Papa, M.A. Results from the first all-sky search for continuous gravitational waves from small-ellipticity sources. *Phys. Rev. Lett.* **2020**, *125*, 171101. [CrossRef]
20. Papa, M.A.; Ming, J.; Gotthelf, E.V.; Allen, B.; Prix, R.; Dergachev, V.; Eggenstein, H.B.; Singh, A.; Zhu, S.J. Search for Continuous Gravitational Waves from the Central Compact Objects in Supernova Remnants Cassiopeia A, Vela Jr., and G347.3–0.5. *Astrophys. J.* **2020**, *897*, 22. [CrossRef]
21. Steltner, B.; Papa, M.; Eggenstein, H.B.; Allen, B.; Dergachev, V.; Prix, R.; Machenschalk, B.; Walsh, S.; Zhu, S.; Kwang, S. Einstein@Home all-sky search for continuous gravitational waves in LIGO O2 public data. *arXiv* **2020**, arXiv:2009.12260.
22. Zhang, Y.; Papa, M.A.; Krishnan, B.; Watts, A.L. Search for Continuous Gravitational Waves from Scorpius X-1 in LIGO O2 Data. *Astrophys. J. Lett.* **2021**, *906*, L14. [CrossRef]
23. Xu, R.; Gao, Y.; Shao, L. Precessions of Spheroidal Stars under Lorentz Violation and Observational Consequences. *arXiv* **2020**, arXiv:2012.01320.
24. Van Den Broeck, C. The Gravitational wave spectrum of non-axisymmetric, freely precessing neutron stars. *Class. Quant. Grav.* **2005**, *22*, 1825–1840. [CrossRef]
25. Gao, Y.; Shao, L.; Xu, R.; Sun, L.; Liu, C.; Xu, R.X. Triaxially-deformed Freely-precessing Neutron Stars: Continuous electromagnetic and gravitational radiation. *Mon. Not. Roy. Astron. Soc.* **2020**, *498*, 1826–1838. [CrossRef]
26. Landau, L.D.; Lifshitz, E.M. *Mechanics*; Butterworth-Heinemann: Oxford, UK, 1976. [CrossRef]
27. Poisson, E.; Will, C.M. *Gravity: Newtonian, Post-Newtonian, Relativistic*; Cambridge University Press: Cambridge, UK, 2014. [CrossRef]
28. Chandrasekhar, S.; Lebovitz, N.R. The Potentials and the Superpotentials of Homogeneous Ellipsoids. *Astrophys. J.* **1962**, *136*, 1037. [CrossRef]
29. Owen, B.J. Maximum elastic deformations of compact stars with exotic equations of state. *Phys. Rev. Lett.* **2005**, *95*, 211101. CrossRef]

30. Goldreich, P. Neutron Star Crusts and Alignment of Magnetic Axes in Pulsars. *Astrophys. J. Lett.* **1970**, *160*, L11. [CrossRef]
31. Jones, D.; Andersson, N. Gravitational waves from freely precessing neutron stars. *Mon. Not. Roy. Astron. Soc.* **2002**, *331*, 203. [CrossRef]
32. Zanazzi, J.; Lai, D. Electromagnetic Torques, Precession and Evolution of Magnetic Inclination of Pulsars. *Mon. Not. Roy. Astron. Soc.* **2015**, *451*, 695–704. [CrossRef]
33. Gao, Y.; Shao, L. Precession of triaxially deformed neutron stars. *arXiv* **2020**, arXiv:2011.04472.